Superdiffusion and heterogeneous dynamics in liquid crystals by microrheology

Fabián García Daza[a], Antonio M. Puertas[b], Alejandro Cuetos[a,c] and Alessandro Patti[d,e,f]

[a] Department of Physical, Chemical and Natural Systems, Pablo de Olavide University, Sevilla, Spain
[b] Department of Chemistry and Physics, University of Almería, 04120 Almería, Spain
[c] Center for Nanoscience and Sustainable Technologies (CNATS), Pablo de Olavide University, Seville, Spain
[d] Department of Applied Physics, University of Granada, 18071 Granada, Spain
[e] Carlos I Institute of Theoretical and Computational Physics, Fuente Nueva s/n, 18071 Granada, Spain
[f] Department of Chemical Engineering, The University of Manchester, Oxford Road, Manchester, M13 9PL, United Kingdom

ARTICLE HISTORY
Compiled August 9, 2024

ABSTRACT
Microrheology (MR) has emerged as a powerful tool for unraveling the intricate local viscoelastic properties of various soft materials. By tracking the free (passive MR) or forced (active MR) diffusion of a tracer, valuable insights into the mechanical characteristics of the host system can be obtained. In this study, we investigate the forced diffusion of a spherical tracer within isotropic and smectic liquid crystal phases of hard rod-like particles. Our findings reveal superdiffusive behaviour induced by external forces, particularly pronounced when these are aligned parallel to the nematic director. Analysis of dynamical susceptibility unveils heterogeneities strongly correlated with the magnitude and orientation of applied forces, highlighting the system's critical dependence on structural ordering. Intriguingly, we observe that tracer superdiffusion, driven by external forces and evident across all relevant system directions, does not demonstrate a strong correlation with resulting dynamical heterogeneities.

KEYWORDS
Liquid crystals; colloids; diffusion; microrheology; Monte Carlo simulation.

1. Introduction

Liquid crystals (LCs) represent states of matter where the directional characteristics of particles (at either colloidal or molecular scales) result in a partial spontaneous disruption of spatial symmetries within the system [1]. This phenomenon gives rise to properties that bridge the gap between crystalline solids and isotropic fluids. Specifically, smectic LCs are distinguished by their layered structures composed of rod-like or disk-like particles. Within these layers, particles tend to align parallel to one an-

CONTACT A. Patti. Email: apatti@ugr.es

other, following a common direction known as the nematic director $\hat{\mathbf{n}}$, thus exhibiting significant orientational order. Positional order is prevalent in the direction parallel to $\hat{\mathbf{n}}$, while being negligible within the layers. This allows particles to move relatively freely, similar to a fluid. Smectic LCs find diverse applications in fields such as displays, sensors, and materials science, owing to their capacity for controlled phase transitions and their display of optical anisotropy.

At the colloidal scale, which is the focus of this study, Onsager's seminal research unveiled the entropy-driven transition from isotropic (I) to nematic (N) phases in systems comprised of infinitely long hard rods, representing a pivotal breakthrough in the field [2]. This landmark discovery was later validated by computer simulations in systems containing perfectly aligned or freely rotating hard rods of finite lengths, unveiling the emergence of thermodynamically stable smectic phases driven by merely entropic effects [3, 4]. Since then, extensive research has deepened our understanding of the equilibrium properties of smectic LCs. A wide array of studies, spanning experimental [5, 6, 7], theoretical [8, 9, 10, 11], and computational [12, 13, 14, 16] approaches, have meticulously analysed the phase behaviour and structural intricacies of smectic LCs formed by colloidal hard rods. Moreover, research efforts have expanded to encompass mixtures of rods with varying geometries [17, 18, 19, 20, 22], as well as mixtures of rods with other types of anisotropic [23] or spherical [24, 25] particles.

Following these preliminary insights into phase behaviour, a still-vibrant interest developed around the dynamics of smectic LCs, mostly sparked by the seminal work by Lettinga and Grelet. Employing video fluorescence microscopy, these researchers investigated the self-diffusion dynamics of rod-like viruses through smectic layers [26]. Their findings unveiled non-Gaussian diffusion patterns and revealed a quasi-quantized layer-to-layer hopping across an energy barrier induced by the smectic layers, a phenomenon, also known as permeation, initially theorized by Helfrich in the 1960s [27]. This work sparked further research that eventually elucidated the impact of caging, clustering and cooperative motion in the relaxation dynamics of smectics [28, 30, 31, 32, 33, 34, 35, 36, 37].

Integrating insights into the phase behaviour, structure, and dynamics of smectics into a framework where microrheology (MR) assumes a central role is key in enhancing our comprehension of how orientational and positional ordering influence the viscoelastic properties of this captivating liquid crystal phase [38, 39]. MR enables the evaluation of the viscoelastic properties of soft materials by monitoring and analysing the dynamics of a guest tracer (or probe particle) that induces, over its characteristic length scales, local deformations in the host fluid [40]. This sets it apart from macroscopic rheology, which examines the material's response across significantly larger length scales. Active MR allows one to picture both the linear and nonlinear viscoelastic domains, unveiling intriguing phenomena like force thinning, where the effective friction coefficient diminishes as the applied force magnitude increases [41]. In contrast, passive MR, which correlates tracer free diffusion with the system's thermal fluctuations, solely offers insight into the linear viscoelastic response. In our recent study, we employed active MR to investigate how the size of the tracer and the direction of an external force impact the effective friction coefficient of smectic LCs of hard rods [39]. Specifically, we demonstrated that the effective friction coefficient maintains a constant value when probed by the tracer at both small and large forces, and reveals a force-thinning nonlinear regime at intermediate forces. We notice that MR has also been applied to study the viscoelastic properties of nematic LCs in the bulk [42] and under confinement [43] by theory and simulations. An experimental work on lyotropic smectic LCs - lamellar phases formed by amphiphilic molecules - highlighted the dif-

ferences from bulk rheology, revealing that the latter remains the preferred technique for assessing macroscopic relaxations over long time scales [44].

Building on these introductory considerations, our focus turns to exploring the forced diffusion of a spherical tracer within smectic LCs of hard rods. Investigating the dynamics of such a tracer not only offers insights into the material's rheology, but also lays the groundwork for understanding the diffusion of small particles or macromolecules in densely packed colloidal suspensions — a multidisciplinary challenge with far-reaching implications [45, 46, 47]. Notably, the presence of long-range ordering, an intrinsic signature of LCs, has been demonstrated to be pivotal in this context [48]. By employing active MR and dynamic Monte Carlo simulation, we unveil a force-induced superdiffusive behaviour where the tracer's mean squared displacement deviates from linear growth over time, instead following a power-law relationship of the form $r^2(t) \propto t^\alpha$, with $\alpha > 1$. Our study extends to the analysis of dynamic heterogeneities, which are found to be strongly correlated with both the magnitude and direction of the applied force.

This work is dedicated to the memory of Prof. Luis Felipe Rull Fernández, whose profound contributions to the field of liquid crystals are deeply missed since his passing in February 2022.

2. Model and simulation method

Our model of colloidal suspensions consists of $N_r = 1440$ rods, modeled as hard spherocylinders, in I and smectic (Sm) liquid-crystal phases, accompanied by $N_t = 1$ hard spherical tracer. The bath particles have an aspect ratio of $L^* = L/\sigma = 5$, where L is the length and σ is the diameter of a cylindrical body capped by hemispherical ends, each with a diameter of σ. The tracer particle is modeled as a sphere with a diameter $d_t = \sigma$. Our simulations incorporate inter-particle interactions through a hard-core potential. Length, energy, and time are given in units of σ, $k_\mathrm{B}T$, and $\tau = \sigma^2/D_0$, respectively, where k_B is Boltzmann's constant, T the absolute temperature, $D_0 = k_\mathrm{B}T/(\eta_s\sigma)$ a diffusion constant, and η_s the viscosity of the implicitly-modelled solvent. The primary focus of this study is the dynamical response of the tracer particle to an external constant force $\mathbf{F}$ pulling it through the host fluid.

Before performing dynamic Monte Carlo (DMC) simulations to study the system's dynamics, a series of Monte Carlo (MC) simulations in the canonical ensemble were performed to equilibrate the systems at a volume fraction of $\phi = 0.349$ and 0.507, corresponding to stable I and Sm phases, respectively [55]. The volume fraction is defined as $\phi = (N_r v_r + N_t v_t)/V$, where $v_r = \pi\sigma^3/6 + \pi\sigma^3 L^*/4$, $v_t = \pi d_t^3/6$, and $V = L_x \times L_y \times L_z$ refers, respectively, to the rod, tracer, and simulation box volumes. We used orthogonal simulation boxes with periodic boundaries. Specifically, I phases were simulated in cubic boxes of size $L_x = L_y = L_z = 26.36\sigma$, whereas Sm LCs in elongated boxes with $L_x \times L_y \times L_z = 31.42 \times 20 \times 20\sigma^3$. Inter-particle interactions are mediated *via* a hard-core potential, and attempted moves are always accepted unless an overlap occurs. Overlaps between rods are detected using the algorithm proposed by Vega and Lago [56]. Equilibration is run in the NPT ensemble until the nematic (S_2) and smectic (λ) order parameters reached steady values within statistical fluctuations. The nematic order parameter is obtained from the diagonalisation of the symmetric

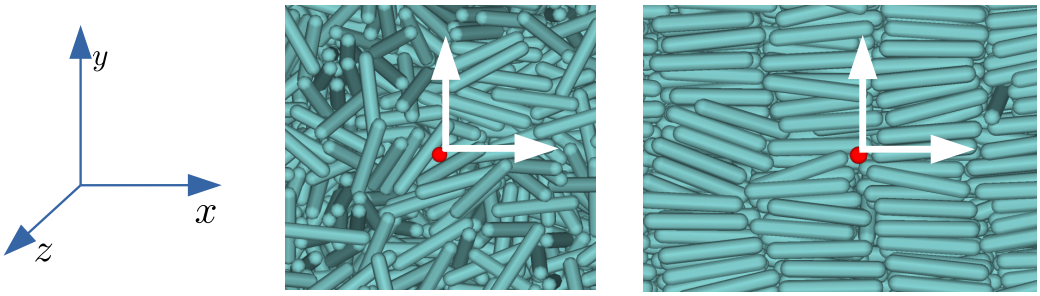

Figure 1. Snapshots of the system in the isotropic (left) and smectic (right) states with reference axes. The white arrows show the two directions of the external force pulling the tracer. Note that the nematic director, $\hat{\mathbf{n}}$, is aligned with the x-axis.

tensor $\mathbf{Q}$, given by:

$$\mathbf{Q} = \frac{1}{2N_r} \sum_{j=1}^{N_r} (3\hat{\mathbf{u}}_j \hat{\mathbf{u}}_j - \mathbf{I}) \tag{1}$$

where $\hat{\mathbf{u}}_j$ is the unit vector aligned with the main axis of rod j and $\mathbf{I}$ the second-rank unit tensor. The largest eigenvalue resulting from the diagonalisation of $\mathbf{Q}$ provides the order parameter S_2, while the corresponding eigenvector gives the nematic director $\hat{\mathbf{n}}$. The smectic order parameter is given by:

$$\lambda = \max_l \left\langle \frac{1}{N_r} \left| \sum_{j=1}^{N_r} e^{2\pi i \mathbf{r}_j \cdot \hat{\mathbf{n}}/l} \right| \right\rangle \tag{2}$$

In our equilibrium MC simulations, we obtained very low values of both order parameters in the I phase, whereas $S_2 \approx 0.9$ and $\lambda \approx 0.8$ in the presence of a Sm phase. In this case, the nematic director was aligned with the x-axis (see Fig. 1). The incorporation of the tracer particle did not have a tangible effect on the values of the order parameters or on the long-range structure of the host phase [39]. Subsequently, the equilibrium configurations obtained were utilized to perform production DMC simulations in the canonical ensemble.

The DMC method simulates Brownian motion of the system's particles by displacing and, in case of rods, rotating selected random particles according to the standard Metropolis algorithm. However, unphysical moves such as jumps, swaps, or cluster moves are not allowed to obtain more realistic trajectories. In the following, we review relevant aspects of DMC for this study, and additional details can be found in Refs. [49, 50, 51, 52, 53, 54]. In a DMC cycle, $N = N_r + N_t$ independent random attempts are made to displace and rotate particles, with rotations being exclusive for rods. Moves are accepted or rejected according to a Metropolis algorithm with probability $\min[1, e^{-\beta \Delta E}]$, where $\beta \equiv (k_\mathrm{B}T)^{-1}$ and ΔE is the change in energy due to particle movement. This change in energy ΔE includes both the interaction with other particles and the work done by the external force, $\mathbf{F} \cdot \delta \mathbf{r}_t$, where $\delta \mathbf{r}_t$ is the displacement of the tracer particle as described below. For rod particle displacement, the position is

updated by decoupling into three contributions $\delta\mathbf{r}_r = X_\parallel \hat{\mathbf{u}}_r + X_{\perp,1}\hat{\mathbf{v}}_{r,1} + X_{\perp,2}\hat{\mathbf{v}}_{r,2}$, where $\hat{\mathbf{u}}_r$ is a unit vector parallel to the main rod axis, while $\hat{\mathbf{v}}_{r,1}$ and $\hat{\mathbf{v}}_{r,2}$ are unit vectors perpendicular to $\hat{\mathbf{u}}_r$ and to each other. The magnitude of displacement is randomly selected from uniform distributions, satisfying $|X_\parallel| \leq \delta r_\parallel$ and $|X_{\perp,m}| \leq \delta r_\perp$, with $m = \{1, 2\}$. The maximum displacements are linked to translational diffusivities at infinite dilution through equations:

$$\delta r_\parallel = \sqrt{2D_{r,\parallel}\delta t_{\mathrm{MC},r}} \tag{3}$$

$$\delta r_\perp = \sqrt{2D_{r,\perp}\delta t_{\mathrm{MC},r}} \tag{4}$$

where $\delta t_{\mathrm{MC},r}$ is the rod's time step in the MC time scale, while $D_{r,\parallel}$ and $D_{r,\perp}$ are, respectively, the diffusion coefficients in the direction parallel and perpendicular to the rod longitudinal axis. For rotations, the orientation vector varies as $\delta\hat{\mathbf{u}}_r = Y_{\varphi,1}\hat{\mathbf{w}}_{r,1} + Y_{\varphi,2}\hat{\mathbf{w}}_{r,2}$, with vectors $\hat{\mathbf{w}}_{r,m}$ chosen to be perpendicular to each other and to $\hat{\mathbf{u}}_r$. The magnitude of the rotations satisfies $|Y_{\varphi,m}| \leq \delta\varphi$, where:

$$\delta\varphi = \sqrt{2D_{r,\varphi}\delta t_{\mathrm{MC},r}} \tag{5}$$

where $D_{r,\varphi}$ is the rod's rotational diffusion coefficient at infinite dilution. For the spherical tracer, only translational moves are considered, and the displacement reads $\delta\mathbf{r}_t = X^t_\parallel \hat{\mathbf{u}}_t + X^t_{\perp,1}\hat{\mathbf{v}}_{t,1} + X^t_{\perp,2}\hat{\mathbf{v}}_{t,2}$, where $\hat{\mathbf{u}}_t$ is a unit vector parallel to the applied force, while $\hat{\mathbf{v}}_{t,1}$ and $\hat{\mathbf{v}}_{t,2}$ are unit vectors perpendicular to $\hat{\mathbf{u}}_t$ and to each other. Displacements fulfill conditions $|X^t_\parallel| \leq \delta r^t_\parallel$ and $|X^t_{\perp,m}| \leq \delta r^t_\perp$. Specifically:

$$\delta r^t_\parallel = \sqrt{2D_t\delta t_{\mathrm{MC},t} + \left(D_t\beta F\delta t_{\mathrm{MC},t}\right)^2} \tag{6}$$

$$\delta r^t_\perp = \sqrt{2D_t\delta t_{\mathrm{MC},t}} \tag{7}$$

where $\delta t_{\mathrm{MC},t}$, F and D_t are, respectively, the MC time step, the modulus of the applied force and infinite-dilution diffusion coefficient of the tracer. Translational and rotational diffusion coefficients of rod-like particles are calculated from analytical expressions derived from the induced-force method [57]:

$$\frac{D_{r,\perp}}{D_0} = \frac{\ln(2/\epsilon) - 1/2 - I^{tt}}{2\pi/\epsilon} \tag{8}$$

$$\frac{D_{r,\parallel}}{D_0} = \frac{\ln(2/\epsilon) - 3/2 - I^{tt}}{\pi/\epsilon} \tag{9}$$

$$\frac{D_{r,\varphi}}{D_0} = 3\frac{\ln(2/\epsilon) - 11/6 - I^{rr}}{\pi\sigma^2/\left(2\epsilon\right)^3} \tag{10}$$

where $\epsilon^{-1} = 2(L^* + 1)$, $I^{tt} = \frac{1}{2}\int_{-1}^{1} \ln h(x)dx$, $I^{rr} = \frac{3}{2}\int_{-1}^{1} x^2 \ln h(x)dx$, with $h(x) = (1-2x^{2n})^{1/2n}$ a parametric function that models particles with symmetry of revolution. The geometry of a spherocylinder is well reproduced by taking $n = 8$. Consequently $I^{tt} \simeq -0.0061$, and $I^{rr} \simeq -0.017$.

The diffusion coefficient of the spherical tracer is estimated from the Stokes-Einstein

equation:

$$\frac{D_t}{D_0} = \frac{1}{3\pi}\frac{\sigma}{d_t} \tag{11}$$

Maximum displacements and rotations of particles are set by rod and tracer time steps, $\delta t_{\mathrm{MC},r}$ and $\delta t_{\mathrm{MC},t}$. Following recent work [54], the time steps of bath and tracer particles are related through their acceptance rates by the following relationship:

$$\delta t_{\mathrm{BD}} = \frac{\mathcal{A}_r}{3}\delta t_{\mathrm{MC},r} = \frac{1}{3}\left(\frac{3}{2}\mathcal{A}_t - \frac{1}{2}\right)\delta t_{\mathrm{MC},t} \tag{12}$$

Here, δt_{BD} is the elementary time step in the BD scale, and $\mathcal{A}_r$ and $\mathcal{A}_t$ are the acceptance rates of bath and tracer particles, respectively. For Eq. 12 to be valid, the condition $\beta F \delta r_{\parallel}^{t} \ll 1$ must be fulfilled [54]. This indicates that, according to Eq. 6, for small forces, the MC time step of the tracer can fall within a wide range of values, while for large forces, the value of the time step is accordingly smaller.

In order to characterise the dynamics of the system under study, several dynamic variables have been calculated. All of them have been obtained by averaging over 500 independent trajectories to improve statistics. Among these, the primary observable analysed is the mean square displacement (MSD) of the spherical tracer (t). To ensure accurate assessment and eliminate the influence of drift induced by the applied force, the MSD has been adjusted by subtracting the average displacement of the tracer particle:

$$\mathrm{MSD} = \langle \Delta\mathbf{r}^2(t)\rangle = \langle[(\mathbf{r}^t(t) - \mathbf{r}^t(0)) - (\mathbf{r}^t(t) - \mathbf{r}^t(0))_{av}]^2\rangle \tag{13}$$

where $(\mathbf{r}^t(t) - \mathbf{r}^t(0))_{av} = \langle \mathbf{r}^t(t) - \mathbf{r}^t(0)\rangle$ is the average displacement at the beginning of each trajectory, angular brackets denote averaging across all trajectories, and $\mathbf{r}^t(t)$ is the vector position of the tracer at instant t. Directional mean square displacements can be defined in a similar manner, also corrected by the average displacement. For instance, the MSD of the tracer in the x-direction can be defined as:

$$\langle \Delta\mathbf{x}^2(t)\rangle = \langle[(x^t(t) - x^t(0)) - (x^t(t) - x^t(0))_{av}]^2\rangle \tag{14}$$

with $x^t(t)$ the x-component of vector $\mathbf{r}^t(t)$. Analogous definitions can be formulated for the y and z components of the tracer displacement. From the MSDs defined in equations 13 and 14, valuable insights into the dynamical regime of the spherical tracer in the fluid of rods can be gleaned. For instance, one can calculate the instantaneous power-law exponent α of the MSD as a function of time as:

$$\alpha = \frac{\partial \ln\langle(\Delta\mathbf{r})^2\rangle}{\partial \ln t} \tag{15}$$

The parameter α furnishes fundamental insights into the motion of the tracer within the fluid of rods. When $\alpha = 1$, the tracer exhibits diffusive behaviour, indicating that its displacement, after accounting for the drift induced by external forces, is primarily

governed by Brownian motion. Conversely, when $\alpha < 1$, the regime is classified as subdiffusive, i.e. the particle's diffusion is slower than in an ideal Brownian scenario. Finally, if $\alpha > 1$, the tracer particle enters the realm of superdiffusive behaviour. In practical scenarios, the tracer's motion often transitions between these regimes over time.

Further insights into the dynamics of the tracer particle are provided by the long-time diffusion coefficient, denoted as D_s. This coefficient is directly related to the slope of the MSD at long times:

$$D_s = \lim_{t\to\infty} \frac{1}{2d} \frac{\partial \langle (\Delta \mathbf{r})^2 \rangle}{\partial t} \tag{16}$$

where d is the dimensionality of interest.

To obtain more information on the origin of the different regimes in the tracer diffusion, we have also calculated some observables that allow us to study the possibility of heterogeneous dynamics in the system. However, given that our setup includes only a single tracer in the system, aimed at circumventing tracer-tracer correlations, investigating dynamic heterogeneities entails analyzing numerous tracer trajectories. This shift necessitates the transition from the typical calculation of observables via an *ensemble average* to a *trajectory average* approach. In particular, the tracer correlation function of a single trajectory, $\Phi_q^t(t)$, is defined as $\Phi_q^t(t) = \cos\left[\mathbf{q} \cdot (\Delta \mathbf{r})\right]$. The values of interest of the wavevector $\mathbf{q}$ correspond to the peaks observed in the tracer-rod static structure factor, defined as

$$S(q) = \frac{1}{N_r N_c} \sum_{i=1}^{N_r} \sum_{j=1}^{N_c} \exp(-i\mathbf{q} \cdot (\mathbf{r}_i - \mathbf{r}^t)) \tag{17}$$

where the first summation is performed over all N_r rod particles, and the second over N_c independent configurations. We stress that the structure factor is calculated for the equilibrium case, $F = 0 k_\mathrm{B} T/\sigma$ and it is therefore a real quantity. The tracer intermediate scattering function is calculated as the trajectory average of the tracer correlation function of a single trajectory, $\langle \Phi_q^t(t) \rangle$. The susceptibility can be calculated then as the standard deviation of the intermediate scattering function over different realisations [58], in our case, different trajectories:

$$\chi_{4,q}(t) = \langle \left[\Phi_q^t(t)\right]^2 \rangle - \langle \Phi_q^t(t) \rangle^2 \tag{18}$$

The susceptibility function analyses how variable is the trajectory of the tracer up to time t in different realisations. Previous results have shown that $\chi_{4,q}(t)$ features a peak in the time regime where the correlation function decays more strongly. The analysis of dynamical heterogeneities has led in many works to identify clusters of particles, or regions, with different mobility. However, in our study, this is not the case since Eq. 18 applies to a single tracer particle. Here, $\chi_{4,q}(t)$ allows us to analyse the extent of differences among various trajectories in relation to the average behaviour. These differences may suggest the presence of distinct transport mechanisms for the tracer and hence of single-particle dynamic heterogeneities.

3. Results

In this section, we analyse the dynamics of a tracer introduced into a bath of spherocylinders, exploring two distinct states: the isotropic phase and the smectic phase. Very recently, we investigated the potential distortion of bath particles surrounding the tracer [54, 39]. In Sm phases, when the applied force aligns parallel to the nematic director and reaches sufficient intensity, it induces microstructural deformation in the particle distribution around the probe, albeit not extending to longer length scales. Under higher forces, a soft layer of rods forms ahead of the tracer, with a particle-free wake developing behind it. Our calculations also reveal minimal coordinated ordering of rods due to the dense packing of the Sm phase. These rods are uniformly oriented and layered, efficiently dissipating energy from the tracer and limiting significant rotation. Attempts to rotate the rods are promptly counteracted by neighboring particles, resulting in modest reorientation. Conversely, when the tracer is forced to move perpendicularly to the nematic director, deforming the surrounding microstructure becomes more challenging, requiring higher forces to observe local distortion. We also notice that significantly larger colloidal spheres can induce more significant distortions in Sm phases, with formation of intriguing Saturn-ring defects and onion-like structures [59]. In the Sm phase, two cases have been studied, as the tracer experiences forces along or perpendicular to the x-axis, which is aligned with the nematic director, as previously noted. Our analysis reveals a superdiffusive behaviour at intermediate times for both states and in both pulling directions. Additionally, we investigate the heterogeneities in tracer dynamics, examining them as potential precursors to superdiffusion.

The simplest observable for the tracer dynamics is its mean squared displacement (MSD), shown in Fig. 2 for the isotropic (top panel) and smectic phases (recall that the MSD is corrected by the tracer average displacement). In the smectic state, we depict the tracer displacement along the x-axis and in the y-axis in separate panels, in order to discern the motion along directions parallel or perpendicular to the nematic director, $\hat{\mathbf{n}}$. In the isotropic state, on the other hand, only the global MSD in the three directions is studied. Note that short time diffusion stems directly from the DMC microscopic dynamics, implying the absence of a short-time ballistic regime.

For zero force, the tracer MSD shows a mild transition from short to long time diffusion at intermediate times in both states and in both directions in the smectic phase, corresponding to a transient caging of the tracer. However, upon increasing the force, a superdiffusive regime emerges, characterised by a time window that shifts towards earlier stages as the force magnitude increases. In this superdiffusive regime the MSD grows faster than linear, reaching quadratic behaviour for the largest forces (the exponent of the MSD vs. time curve is shown in Fig. 3). This transient regime is consistently observed across all cases, transitioning into long-time diffusion, with the exception being the largest perpendicular force in the smectic bath, where sufficiently long times might not have been reached. This suggests a significant enhancement in tracer diffusion for all force orientations, a phenomenon that we further discuss in the subsequent analysis. It must be stressed that previous works of tracers in the smectic phase found that the tracer moves preferentially within the interlayer planes. Here, we find that for large forces, the tracers indeed seeps into the layers in a superdiffusive regime, not only when it is pulled in the x direction, but also when the forcing acts within the yz-plane. Finally, it's worth noting that this entire phenomenology remains consistent even when the force forms an angle with the nematic director, a case which is not explicitly shown but corroborates the observed dynamics.

The stationary points (maximum or minimum) of the exponent of the MSD vs.

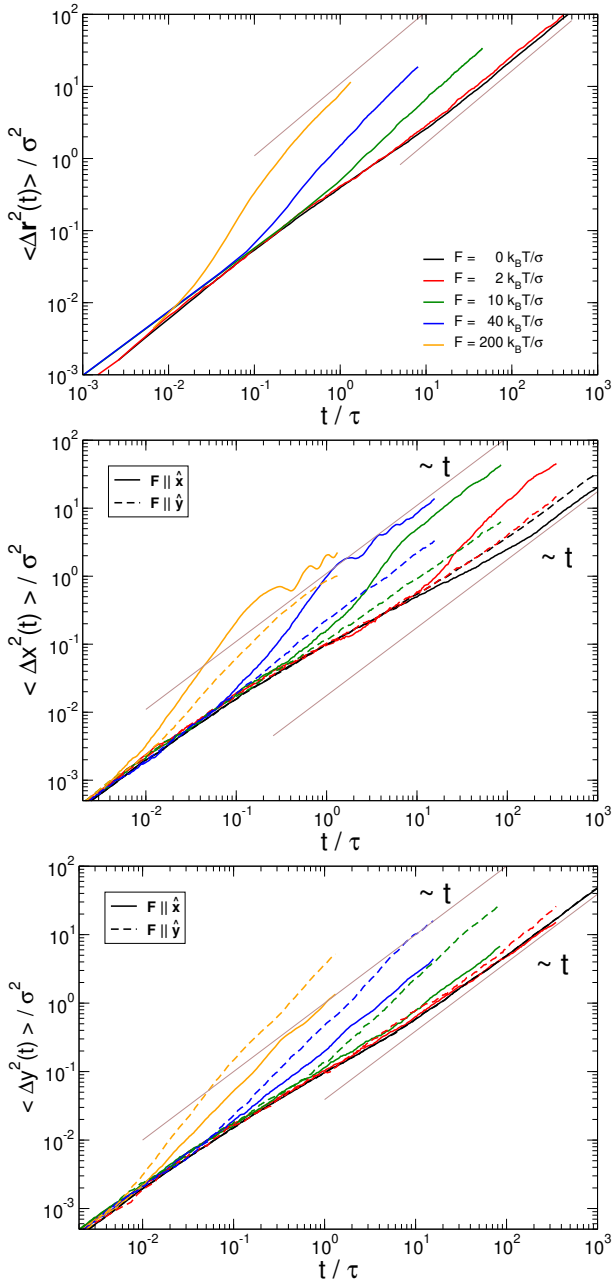

Figure 2. Tracer mean squared displacement for different states and directions, as labeled. The bath is in the isotropic phase (top panel), or in the smectic phase (intermediate and bottom panels). The continuous lines show the MSD contributions for forces parallel to the nematic director, and dashed lines in the perpendicular direction. We remind that the nematic director is parallel to the x-axis. Straight lines indicate the dependence of the MSD on time at short and long timescales.

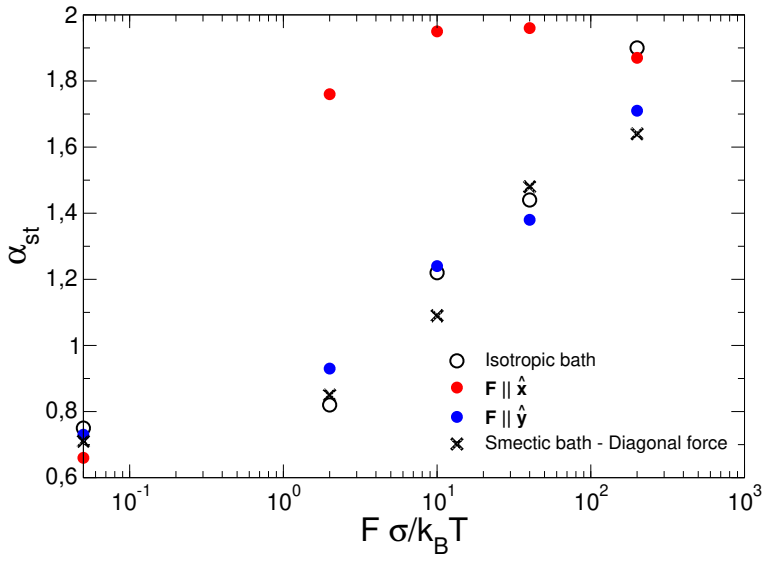

Figure 3. Exponent of the tracer MSD parallel to the force for different cases, as labeled. Empty circles represent the MSD exponent measured in the isotropic bath. Red and blue circles indicate the MSD exponent measured parallel and perpendicular to the nematic director of the smectic bath, respectively. Crosses denote forces at a 45° angle to the nematic director of the smectic phase. Data from passive microrheology ($F = 0$) are also included on the vertical axis.

time curve, α_{st}, is plotted as a function of the force for all cases in Fig. 3. For passive microrheology, where no external force is applied, and for small forces, the occurrence of superdiffusion is not observed. Instead, a subdiffusive regime emerges, indicating the caging of the tracer in dense states. Consequently, in such cases, the stationary exponent associated with this behaviour falls below one. For larger forces, the exponent increases, eventually reaching a value of 2 for the smectic bath with a force applied along the x-direction. However, for forces applied perpendicular to or diagonally with respect to the nematic director, the trend mirrors that of the isotropic bath, with the exponent approaching quadratic behaviour only for extremely large forces.

The long-time motion of the tracer pulled in the x-direction is modulated by the LC layers, resulting in the "ripples" of the MSD observed for the largest forces in the middle panel, and more clearly in Fig. 4, which plots the MSD corrected by the long time diffusive motion, $\sim 2D_s t$. In various trajectories, when a sufficiently strong force is applied, the tracer is propelled into the layer within comparable time scales, resulting in in-phase oscillations. This is corroborated by the tracer's position, as depicted in Fig. 4 (thin lines), where we observe that the MSD exhibits a faster-than-linear trend when the tracer displaces below the constant velocity trend. Conversely, $\langle \Delta x^2(t) \rangle$ demonstrates sub-linear growth when the tracer moves above it.

This phenomenology is obviously absent for the isotropic bath, and when the force is perpendicular to the layers (the tracer is pulled within the inter-layers y direction), but also for small forces parallel to the nematic director. In the latter case, the tracer does not explore the inner parts of the layers (for too small forces), or this exploration is performed in an incoherent way, resulting in a simple linear growth of the longitudinal MSD. In any case, it can explain the transient superdiffusive regime at intermediate times as the coherent motion of tracers, and points that the arrangements of the structure at the microscopic level is responsible for superdiffusion, in our system. It must be mentioned, nevertheless, that superdiffusion was first reported in

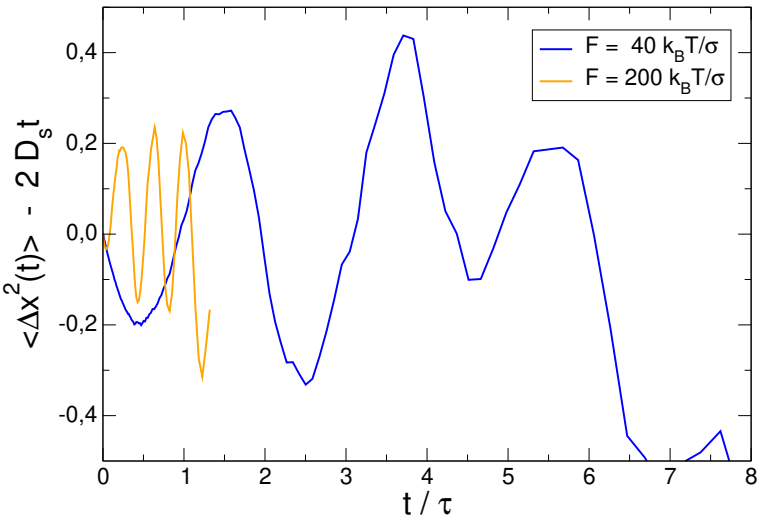

Figure 4. Deviations of the tracer mean squared displacement from linear behaviour in the nematic bath with the force parallel to the nematic director, for the two largest forces studied. The thin lines show the corrected tracer position for the same color code.

undercooled fluids of Yukawa particles, with no structure [60, 61], and also observed in other structureless systems of spheres, such as the low density Lorentz gas [62]. In all cases, though, it appears as a transient regime between short time dynamics and long time diffusion.

The tracer self-diffusion coefficients, obtained from the slope of the long time linear growth of the MSD, are shown in Fig. 5. In all cases, this increases with the external force, but it is maximal for the isotropic bath, as expected, and reaches a plateau at large forces. This trend is inverse to that of the effective friction coefficient obtained from the steady tracer velocity [39], although the Stokes-Einstein relation should not be expected to hold for these far-from-equilibrium systems (particularly at large forces). In any case, the tracer self-diffusion coefficient or the effective friction coefficient indicate an important force-thinning regime, similar to the shear-thinning observed in bulk rheology of viscoelastic fluids.

To gain further insight into the origin of this superdiffusion of the tracer, our attention turns to the heterogeneity of its dynamics, using the dynamic susceptibility as defined previously. For this analysis, we must first identify the most relevant wavevectors in the dynamics of the system, studying the tracer-rod structure factor for the isotropic and nematic phases (see Fig. 6). In the isotropic phase, $S(q)$ approaches zero, indicating a lack of characteristic distances due to the low density of rods. In contrast, a negative intense peak is observed in the smectic phase for $q\sigma \sim 1$ and a positive one for $q\sigma \sim 2$, corresponding to distances of $2\pi/q \approx 6$ and 3, respectively. The latter marks the strong tracer-rod correlation in the direction of the nematic vector, at ~ 3, i.e. the LC layers as observed from the interlayer plane. In contrast, the negative peak reports the strong anti-correlation at a distance ~ 6, i.e. the nearest interlayer, where there are no rods. Finally, let us note that in the calculation of these structure factors, all wavevectors compatible with the periodic boundary conditions were selected, but the dominant contribution was from wavevectors parallel to the x direction (i.e. parallel to the nematic director).

Fig. 6 indicates that there is no preferential wavevector for the tracer in the isotropic bath, whereas $q = 1$ is the optimal choice for the smectic case, in the x-direction. Thus

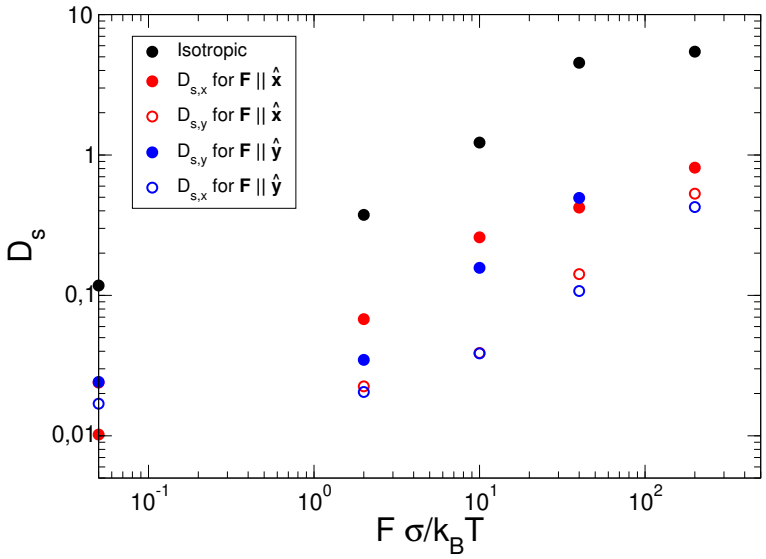

Figure 5. Tracer diffusion coefficients for the different baths and force directions, as labeled, as a function of the external force. As in Fig. 3, the data from passive microrheology are presented in the y-axis.

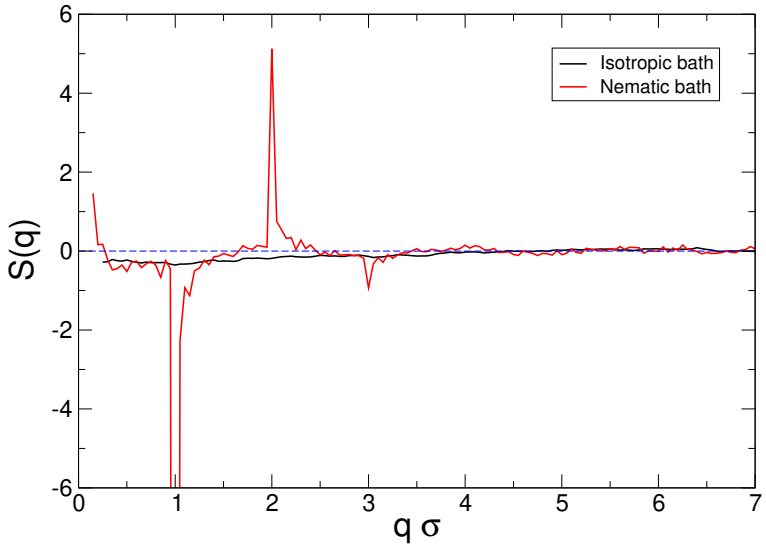

Figure 6. Tracer-rod equilibrium structure factor obtained at $\mathbf{F} = 0 k_{\mathrm{B}}T/\sigma$ for the isotropic and smectic baths, as labeled.

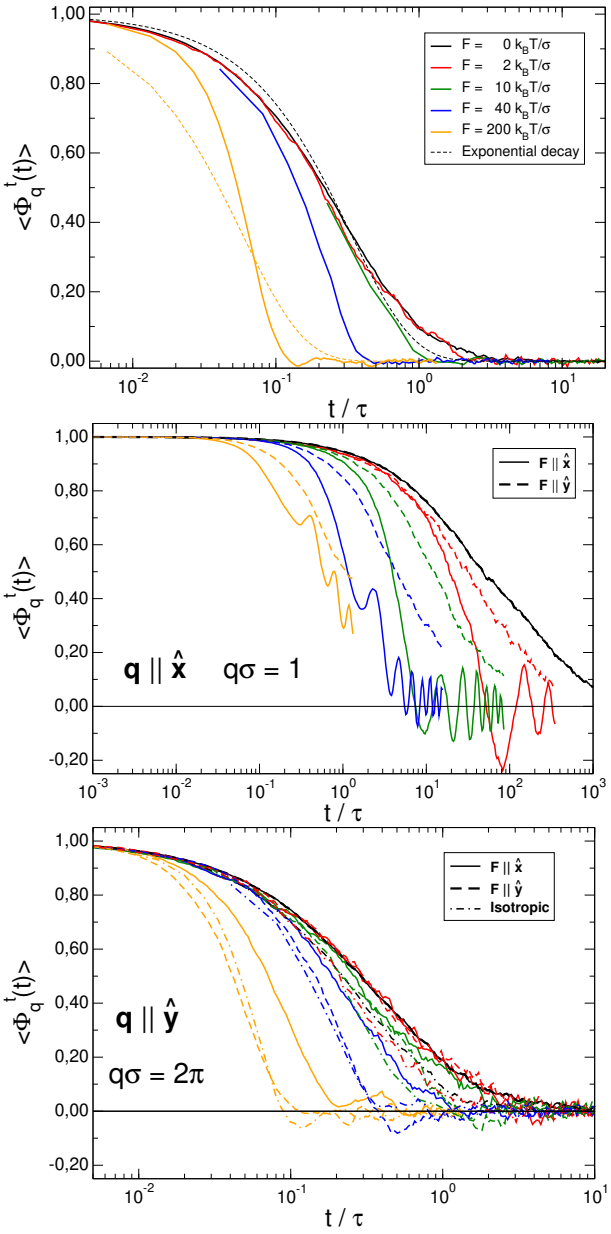

Figure 7. Tracer self-intermediate scattering function for different forces, as labeled. The bath is in the isotropic phase (top panel), or in the smectic phase. The wavevector is parallel to the x-axis with modulus $q\sigma = 1$ in the middle panel. In the bottom panel, the wavevector has modulus $q\sigma = 2\pi/6$ and it is within the yz-plane. Black and orange dashed lines are fits obtained, respectively, at $\mathbf{F} = 0k_{\mathrm{B}}T/\sigma$ and $\mathbf{F} = 200k_{\mathrm{B}}T/\sigma$. In the top panel, the thin dashed lines are exponential fittings to the curves.

we take the standard $q\sigma = 2\pi$ for the dynamics of the tracer in the isotropic case and perpendicular to the nematic director, and $q\sigma = 1$ for the dynamics parallel to the x-axis. In all cases, forces in the x and in the y directions are considered.

Fig. 7 shows the tracer self-intermediate scattering function, as defined above, for the istropic and smectic baths. In the smectic case, wavevectors parallel and perpendicular to the nematic director are shown (middle and bottom panels, respectively), with different moduli. The forces parallel and perpendicular to the nematic director are shown with continuous and dashed lines, respectively. Generically, the application of the external force provokes a faster decay of this correlation function.

In the isotropic bath (top panel), the wavevector modulus is $q\sigma = 2\pi$, as mentioned above. It is worth noticing that although the separation between short-time and long-time diffusion, namely the cage effect, is not observable in the MSD of the unforced tracer, this correlation function decays as a stretched exponential, typical of viscoelastic systems (a simple exponential fitting is presented for comparison, with the dashed lines). For larger forces, on the other hand, the decay is compressed and faster than the simple exponential, corresponding to the superdiffusion regime discussed previously.

In the smectic bath, the dynamics is faster in the direction of the force, as expected, but all correlation functions decay faster for stronger forces. The tracer intermediate scattering function in the smectic bath when the force is parallel to the nematic director shows oscillations, reproducing the ripples in the MSD or the displacement. However, because this function focuses on the relevant length scale, the oscillations are noticeable even for intermediate forces at long times, which was hardly visible in the MSD. On the other hand, in the y-direction, the dynamics of the forced tracer is similar to the isotropic bath, with small differences only for small forces. This indicates that the tracer moves in this region as in an isotropic environment.

Finally, let us note that the relaxation time scale can be obtained from the decay of the correlation function (not shown). This features a behaviour similar to the effective friction coefficient, or the inverse diffusion coefficient, as they all measure, in different ways the same phenomenon.

The dynamical susceptibility, as calculated according to Eqn. (18), quantifies the standard deviation of the tracer's intermediate scattering function. Essentially, it measures the degree of variability among different trajectories. This is shown in Fig. 8 for the same cases as Fig. 7. As previously reported for bulk systems [58], the susceptibility reaches its maximum value when the system undergoes relaxation. Similarly, in our analysis the tracer susceptibility exhibits this characteristic behaviour. Consequently, the peak in $\chi_{4,q}$ shifts towards shorter times with increasing force magnitude across all cases. Furthermore, in the isotropic state, the susceptibility diminishes with increasing forces, indicating a greater similarity among tracer trajectories.

In the smectic bath the tracer dynamical susceptibility is larger than in the isotropic case, and behaves differently. The dynamics in the direction of the nematic director (intermediate panel) depends strongly on the direction of the force; when the force is parallel to $\hat{\mathbf{n}}$, the susceptibility is maximal for intermediate forces, in the force thinning regime, where the diffusion coefficient varies more strongly, and also corresponding to the lowest force where superdiffusion is observed (with an exponent of the MSD close to 2). We interpret this non-monotonic behaviour of the susceptibility function for intermediate forces and when they are parallel to the nematic director as the appearance of the dynamic heterogeneities as we defined them in Section 2. Increasing the force helps the tracer diffuse through the smectic layers, though this is not always observed in all trajectories. These variations in the tracer's diffusion mechanism in smectic fluids lead to dynamic heterogeneities, resulting in an increase in the peak of $\chi_{4,q}(t)$. Upon

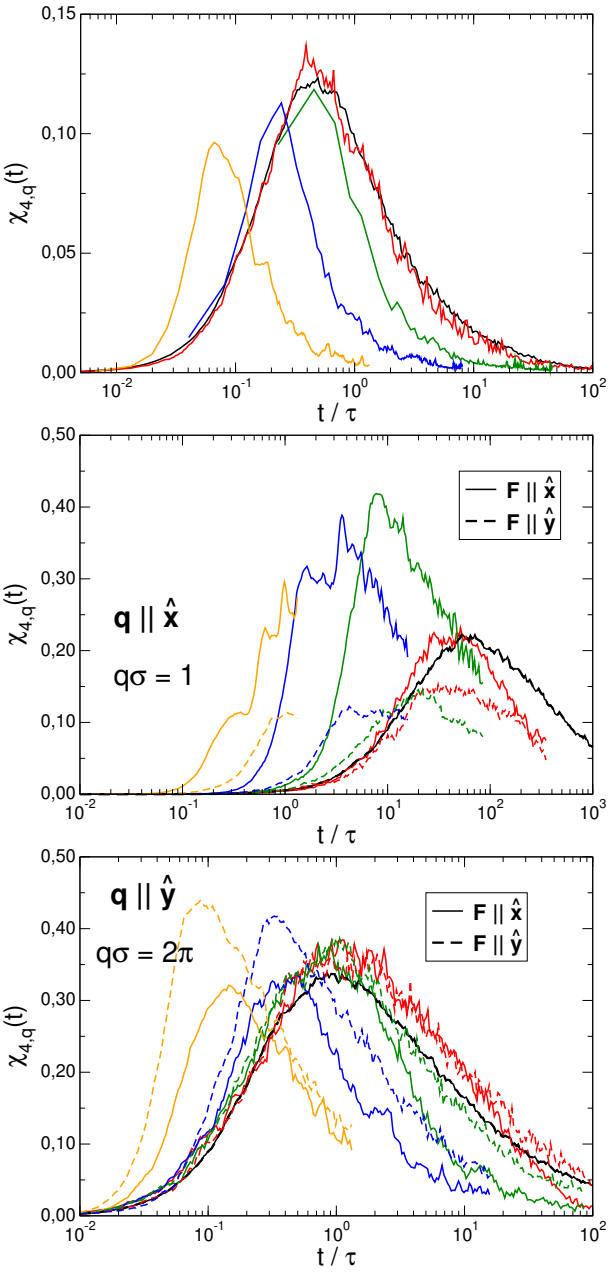

Figure 8. Dynamical susceptibility of the tracer for the same states and forces as Fig. 7 (the lines have the same meaning as that figure).

increasing the force magnitude, more and more trajectories show the tracer moving between layers, making the system dynamics more homogeneous. However, when the force is perpendicular to $\hat{\mathbf{n}}$, the susceptibility decreases upon increasing the force. Notably, the case without force, $F = 0k_{\mathrm{B}}T/\sigma$, lies in between, but even for small forces, this is broken.

For the dynamics in the interlayer planes, $\mathbf{q} \perp \hat{\mathbf{n}}$ (bottom panel), the dynamics shows only mild dependence on the force, with a slight increase when $\mathbf{q}$ is parallel to $\mathbf{F}$, but the values are notably higher than in the isotropic case. It cannot be ruled out that a maximum appears at even larger forces. Indeed, the correlation with superdiffusion in this context appears to be less straightforward.

Finally, let us also note that the overlap correlation function [58] was also translated to tracer dynamics but the results were very similar to those of the self-intermediate scattering function. The dynamical susceptibility was also similar, but its intensity was less sensitive to the tracer dynamics, due to its definition. We have, therefore, shown here only the analysis based on $\langle \Phi_q^t(t) \rangle$ and its dynamical susceptibility.

4. Conclusions

Microrheology has emerged as a valuable technique for probing the mechanical characteristics of complex materials at small scales, particularly in the realms of viscoelasticity and viscoplasticity. In this study, we investigated a system comprised of spherocylinders in both an isotropic state and within the smectic phase, employing a spherical tracer. Our findings reveal a superdiffusive behaviour induced by external forces, notably heightened within the smectic bath, particularly when the force aligns parallel to the nematic director. However, it is remarkable that such behaviour is also observable in other directions and within the isotropic bath. Furthermore, we calculate the dynamical susceptibility to explore the system's heterogeneities, transitioning from ensemble average to trajectory average analysis. The susceptibility results unveil a peak within the timeframe corresponding to the relaxation of the correlation function, notably maximized for intermediate forces aligned parallel to the nematic director. Regardless of force orientation, the tracer's dynamics within the smectic bath exhibit greater heterogeneity compared to the isotropic state.

The analysis of tracer superdiffusion, as depicted in Figs. 2 and 3, in conjunction with the findings from the dynamical susceptibilities discussed earlier, reveals that establishing a definitive correlation between them proves elusive. While superdiffusion, induced by external forces and observable in all directions, is notably clearer when forces align parallel to the nematic director and in the direction of the force, a direct correspondence with dynamical heterogeneities is not straightforward. In instances where superdiffusion is prominent, dynamical heterogeneities reach their peak. Moreover, in the isotropic bath, superdiffusion becomes more pronounced for larger forces, coinciding with a decrease in $\chi_{4,q}$. This trend holds true in the smectic bath when the force aligns parallel to the nematic director, but not when it is perpendicular. Intriguingly, distinct trends emerge for wavevectors oriented in different directions. Notably, for $q\sigma = 1$, a non-monotonic trend is indeed observed.

5. Acknowledgments and Dedication

F.A.G.D. and A.P. acknowledge a María Zambrano fellowship, funded by the NextGenerationEU/PRTR program of the European Union, the Plan de Recuperación, Transformación y Resiliencia, and the Ministerio de Universidades. A.C., A.M.P. and A.P. acknowledge, respectively, grants PPID2021-126121NB-I00, PID2021-127836NB-I00 and PID2022-136540NB-I00 awarded by MICIU/AEI/10.13039/501100011033 and ERDF A way of making Europe. A.P. also acknowledges grant P21_00015 funded by Junta de Andalucía - Consejería de Universidad, Investigación e Innovación. The authors are thankful to the C3UPO of the Pablo de Olavide University for the support with HPC facilities.

All authors would like to dedicate the present work to the memory of Prof. Luis Felipe Rull Fernández, whose profound contributions to the field of liquid crystals are deeply missed since his passing in February 2022.

References

[1] P. G. de Gennes and J. Prost, *The Physics of Liquid Crystals*, (Clarendon, Oxford, 1993).

[2] L. Onsager, *The effects of shape on the interaction of colloidal particles*, Ann. N.Y. Acad. Sci. *51*, 627, **1949**.

[3] A. Stroobants, H. N. W. Lekkerkerker, and D. Frenkel, *Evidence for Smectic Order in a Fluid of Hard Parallel Spherocylinders*, Phys. Rev. Lett. *57*, 1452, **1986**.

[4] D. Frenkel, H. N. W. Lekkerkerker, and A. Stroobants, *Thermodynamic stability of a smectic phase in a system of hard rods*, Nature, *332*, 822, **1988**.

[5] Z. Dogic and S. Fraden, *Smectic Phase in a Colloidal Suspension of Semiflexible Virus Particles*, Phys. Rev. Lett. *78*, 2417, **1997**.

[6] Z. Dogic and S. Fraden, *Development of model colloidal liquid crystals and the kinetics of the isotropic–smectic transition*, Philos. Trans. R. Soc. London, Ser. A *359*, 997, **2001**.

[7] H. Maeda and Y. Maeda, *Liquid Crystal Formation in Suspensions of Hard Rod-like Colloidal Particles: Direct Observation of Particle Arrangement and Self-Ordering behaviour*, Phys. Rev. Lett. *90*, 018303, **2003**.

[8] B. Mulder, *Density-functional approach to smectic order in an aligned hard-rod fluid*, Phys. Rev. A, *35*, 3095, **1987**.

[9] A. M. Somoza and P. Tarazona, *Nematic and smectic liquid crystals of hard spherocylinders*, Phys. Rev. A, *41*,965, **1990**.

[10] D. de las Heras, Y. Martínez-Ratón, and E. Velasco, *Surface and smectic layering transitions in binary mixtures of parallel hard rods*, Phys. Rev. E *81*, 021706, **2010**.

[11] H. H. Wensink and E. Grelet, Phys. Rev. E, *Elastic response of colloidal smectic liquid crystals: Insights from microscopic theory*, *107*, 054604, **2023**.

[12] J. A. Veerman and D. Frenkel, *Phase diagram of a system of hard spherocylinders by computer simulation*, Phys. Rev. A, *41*, 3237, **1990**.

[13] J. M. Polson and D. Frenkel, *First-order nematic-smectic phase transition for hard spherocylinders in the limit of infinite aspect ratio*, Phys. Rev. E *56*, R6260, **1997**.

[14] P. Bolhuis and D. Frenkel, *Tracing the phase boundaries of hard spherocylinders*, J. Chem. Phys. *106*, 666, **1997**.
[15] J. S. van Duijneveldt, A. Gil-Villegas, G. Jackson, M. P. Allen, *Simulation study of the phase behaviour of a primitive model for thermotropic liquid crystals: Rodlike molecules with terminal dipoles and flexible tails*, J. Chem. Phys. *112*, 9092, **2000**.
[16] P. A. Monderkamp, R. Wittmann, M. te Vrugt, A. Voigt, R. Wittkowski, H. Löwen, *Topological fine structure of smectic grain boundaries and tetratic disclination lines within three-dimensional smectic liquid crystals*, Phys. Chem. Chem. Phys. *24*, 15691, **2022**.
[17] G. J. Vroege and H. N. W. Lekkerkerker, *Theory of the isotropic-nematic-nematic phase separation for a solution of bidisperse rodlike particles*, J. Phys. Chem. *97*, 3601, **1993**.
[18] R. van Roij, B. Mulder, M. Dijkstra, *Phase behaviour of binary mixtures of thick and thin hard rods*, Physica A *261*, 374, **1998**.
[19] S. Varga, E. Velasco, L. Mederos, F. J. Vesely, *Stability of the columnar and smectic phases of length-bidisperse parallel hard cylinders*, Mol. Phys., *107*, 2481-2492, **2009**.
[20] I. Kato, K. Sunahara, K. Okoshi, *Smectic–Smectic Phase Segregation Occurring in Binary Mixtures of Long and Short Rigid-Rod Helical Polysilanes*, Macromolecules, *52*, 1134-1139, **2019**.
[21] M. Chiappini, E. Grelet, and M. Dijkstra, *Speeding up Dynamics by Tuning the Noncommensurate Size of Rodlike Particles in a Smectic Phase*, Phys. Rev. Lett. *124*, 087801, **2020**.
[22] G. L. A. Kusters, M. Barella, P. van der Schoot, *Preferential ordering of incommensurate-length guest particles in a smectic host*, J. Chem. Phys. *160*, 084904, **2024**.
[23] J. Camp, M. P. Allen, P. G. Bolhuis, D. Frenkel, *Demixing in hard ellipsoid rod-plate mixtures*, J. Chem. Phys. *106*, 9270, **1997**.
[24] V. F. D. Peters,† A. González García, H. H. Wensink, M. Vis, R. Tuinier, *Multiphase Coexistences in Rod–Polymer Mixtures*, Langmuir, *37*, 11582–11591, **2021**.
[25] J. Opdam, D. Guu, M. P. M. Schelling, D. G. A. L. Aarts, R. Tuinier, M. P. Lettinga, *Phase stability of colloidal mixtures of spheres and rods*, J. Chem. Phys. *154*, 204906, **2021**.
[26] M. P. Lettinga and E. Grelet, *Self-Diffusion of Rodlike Viruses through Smectic Layers*, Phys. Rev. Lett. *99*, 197802, **2007**.
[27] W. Helfrich, *Capillary Flow of Cholesteric and Smectic Liquid Crystals*, Phys. Rev. Lett. *23*, 372 **1969**.
[28] M. Bier, R. van Roij, M. Dijkstra, P. van der Schoot, *Self-Diffusion of Particles in Complex Fluids: Temporary Cages and Permanent Barriers*, Phys. Rev. Lett. *101*, 215901, **2008**.
[29] G. Cinacchi and L. De Gaetani, *Mechanism of diffusion in the smectic-A phase of wormlike rods studied by computer simulation*, Phys. Rev. E *79*, 011706, **2009**.
[30] A. Patti, D. El Masri, R. van Roij, M. Dijkstra, *Stringlike Clusters and Cooperative Interlayer Permeation in Smectic Liquid Crystals Formed by Colloidal Rods*, Phys. Rev. Lett. *103*, 248304, **2009**.
[31] A. Patti, D. El Masri, R. van Roij, M. Dijkstra, *Collective diffusion of colloidal hard rods in smectic liquid crystals: Effect of particle anisotropy*, J. Chem. Phys. *132*, 224907, **2010**.
[32] R. Matena, M. Dijkstra, A. Patti, *Non-Gaussian dynamics in smectic liquid crystals of parallel hard rods*, Phys. Rev. E *81*, 021704, **2010**.

[33] E. Pouget, E. Grelet, and M. P. Lettinga, *Dynamics in the smectic phase of stiff viral rods*, Phys. Rev. E *84*, 041704, **2011**.

[34] L. Alvarez, M. P. Lettinga, E. Grelet, *Fast Diffusion of Long Guest Rods in a Lamellar Phase of Short Host Particles*, Phys. Rev. Lett. *118*, 178002, **2017**.

[35] M. Saito, J. Yamamoto, R. Masuda, M. Kurokuzu, Y. Onodera, Y. Yoda, M. Seto, *Direct observation of interlayer molecular translational motion in a smectic phase and determination of the layer order parameter*, Phys. Rev. Research, *1*, 012008, **2019**.

[36] M. P. Lettinga, L. Alvarez, O. Korculanin, E. Grelet, *When bigger is faster: A self-Van Hove analysis of the enhanced self-diffusion of non-commensurate guest particles in smectics*, J. Chem. Phys. *154*, 204901, **2021**.

[37] D. Cywiak, A. Gil-Villegas, A. Patti, *Long-time relaxation dynamics in nematic and smectic liquid crystals of soft repulsive colloidal rods*, Phys. Rev. E *105*, 014703, **2022**.

[38] F. A. García Daza, A. M. Puertas, A. Cuetos, A. Patti, *Microrheology of isotropic and liquid-crystalline phases of hard rods by dynamic Monte Carlo simulations*, J. Mol. Liq. *365*, 120146, **2022**.

[39] F. A. García Daza, A. M. Puertas, A. Cuetos, A. Patti, *Insight into the Viscoelasticity of Self-Assembling Smectic Liquid Crystals of Colloidal Rods from Active Microrheology Simulations*, J. Chem. Theory Comput. *20*, 1579–1589, **2024**.

[40] T. M. Squires, T. G. Mason, *Fluid mechanics of microrheology*, Annu. Rev. Fluid Mech. *42*, 413–438, **2010**.

[41] T. M. Squires, J. F. Brady, *A simple paradigm for active and nonlinear microrheology*, Phys. Fluids *17*, 073101, **2005**.

[42] M. Gómez-González and J. C. del Álamo, *Two-point particle tracking microrheology of nematic complex fluids*, Soft Matter, *12*, 5758-5779, **2016**.

[43] A. Córdoba, T. Stieger, M. G. Mazza, M. Schoen, J. J. de Pablo, *Anisotropy and probe-medium interactions in the microrheology of nematic fluids.* J. Rheol. *60*, 75–95, **2016**.

[44] M. M. Alam and R. Mezzenga, *Particle Tracking Microrheology of Lyotropic Liquid Crystals*, Langmuir *27*, 6171–6178, **2011**.

[45] K. Biji, C. Ravishankar, C. Mohan, T.K. Srinivasa Gopal, *Smart packaging systems for food applications: a review*, J. Food Sci. Technol. *52*, 6125–6135, **2015**.

[46] H. Wei, Y. Wang, J. Guo, N.Z. Shen, D. Jiang, X. Zhang, X. Yan, J. Zhu, Q. Wang, L. Shao, H. Lin, S. Wei, Z. Guo, *Advanced micro/nanocapsules for self-healing smart anticorrosion coatings*, J. Mater. Chem. A *3*, 469–480, **2015**.

[47] N. Kamaly, B. Yameen, J. Wu, O.C. Farokhzad, *Degradable controlled-release polymers and polymeric nanoparticles: Mechanisms of controlling drug release*, Chem. Rev. *116*, 2602–2663, **2016**.

[48] L. Tonti, F. A. García Daza, A. Patti, *Diffusion of globular macromolecules in liquid crystals of colloidal cuboids*, J. Mol. Liq. *338*, 116640, **2021**.

[49] A. Patti and A. Cuetos, *Brownian dynamics and dynamic Monte Carlo simulations of isotropic and liquid crystal phases of anisotropic colloidal particles: A comparative study*, Phys. Rev. E, *86*, 011403, **2012**.

[50] A. Cuetos and A. Patti, *Equivalence of Brownian dynamics and dynamic Monte Carlo simulations in multicomponent colloidal suspensions*, Phys. Rev. E, *92*, 022302, **2015**.

[51] D. Corbett, A. Cuetos, M. Dennison, A. Patti, *Dynamic Monte Carlo algorithm for out-of-equilibrium processes in colloidal dispersions*, Phys. Chem. Chem. Phys., *20*, 15118-15127, **2018**.

[52] M. Chiappini, A. Patti, M. Dijkstra, *Helicoidal dynamics of biaxial curved rods in twist-bend nematic phases unveiled by unsupervised machine learning techniques*, Phys. Rev. E *102*, 040601(R), **2020**.
[53] F. A. García Daza, A. Cuetos, A. Patti, *Dynamic Monte Carlo simulations of inhomogeneous colloidal suspensions*, Phys. Rev. E, *102*, 013302, **2020**.
[54] F. A. García Daza, A. M. Puertas, A. Cuetos, A. Patti, *Microrheology of colloidal suspensions via dynamic Monte Carlo simulations*, J. Colloid Interface Sci., *605*, 182-192, **2022**.
[55] P. Bolhuis and D. Frenkel, *Tracing the phase boundaries of hard spherocylinders*, J. Chem. Phys., *106*, 666-687, **1997**.
[56] C. Vega and S. Lago, *A fast algorithm to evaluate the shortest distance between rods*, *18*, 55-59, **1994**.
[57] J. Bonet Avalos, J.M. Rubí, D. Bedeaux and G. van der Zwan, *Friction coefficients of axisymmetric particles in suspension*, Phys. A, *211*, 193-217, **1994**.
[58] Coniglio, A., Abete, T., de Candia, A. et al. *A review of the dynamical susceptibility in different complex systems.* Eur. Phys. J. Spec. Top. *161*, 45–54, **2008**.
[59] S. Püschel-Schlotthauer, V. Meiwes Turrión, C. K. Hall, M. G. Mazza, M. Schoen, *The Impact of Colloidal Surface-Anchoring on the Smectic A Phase*, Langmuir *33*, 2222-2234, **2017**.
[60] D. Winter, J. Horbach, P. Virnau, K. Binder, *Active Nonlinear Microrheology in a Glass-Forming Yukawa Fluid*, Phys. Rev. Lett., *108*, 028303, **2012**.
[61] D. Winter, J. Horbach, *Non-linear active micro-rheology in a glass-forming soft-sphere mixture*, J. Chem. Phys. *138*, 12A512, **2013**.
[62] S. Leitmann, S. Mandal, M. Fuchs, A.M. Puertas, Th. Franosch, *Time-dependent active microrheology in dilute colloidal suspensions*, Phys. Rev. Fluids, *3*, 103301, **2018**.